Integrating Materials and Manufacturing Innovation
https://doi.org/10.1007/s40192-023-00310-w

THEMATIC SECTION: ADDITIVE MANUFACTURING BENCHMARKS 2022

Part Deflection Measurements of AM-Bench IN718 3D Build Artifacts

Maxwell Praniewicz[1] · Jason C. Fox[1] · Jared Tarr[1]

Received: 26 July 2023 / Accepted: 7 September 2023

Abstract

One of the primary barriers for adoption of additive manufacturing (AM) had been the uncertainty in the performance of AM parts due to residual stresses/strains. The rapid melting and solidification which occurs during AM processes result in high residual stresses/strains that produce significant part distortion. While efforts to mitigate residual stresses, such as post-process heat treatment, can reduce these effects, they nullify the benefits of the as-built component microstructure. Therefore, the ability to predict as-built component residual stresses and component deflection is crucial. AM-Bench seeks to provide modelers with high-fidelity data in well-characterized AM components to aid in model development and calibration. The measurements reported here are part of the 3D builds of nickel-based superalloy IN718 test objects for the CHAL-AMB2022-01-PD modeling challenges. The part deflection measurements were performed using a coordinate measurement machine after the part was partially separated from the build plate.

Keywords Additive manufacturing · Residual stress · Stress relaxation · Distortion measurement

Introduction

A challenge inhibiting the widespread adoption of engineering alloy components produced by additive manufacturing (AM) is the presence of high residual stresses. These residual stresses are due to high cooling rates and thermal gradients present within the AM process [1]. Presently, there is a need to validate and improve the accuracy of model predictions for residual stresses within AM components. The additive manufacturing benchmark test series (AM-Bench) was developed with the goal of enabling modelers to test their simulations against rigorous, highly controlled additive manufacturing benchmark test data. A description of how these part deflection measurements and other residual stress measurement techniques fit into the larger picture of AM-Bench is provided in the introductory article to this collection [2].

In this work, the part deflection due to residual stress was evaluated for AM samples made from Inconel 718 (IN718), a solid solution hardened nickel-based super alloy. Additional information may also be found on the National Institute of Standards and Technology (NIST) AM-Bench website at https://www.nist.gov/ambench/amb2022-01-benchmark-measurements-and-challenge-problems under section 3.4 Part Distortion and are identified elsewhere as CHAL-AMB2022-01-PD. This document provides a detailed description of the measurement procedure and analysis. This document presents the final measurement results, which can also be found at https://www.nist.gov/ambench/am-bench-2022-challenge-problems-and-measurement-results by clicking the link to the measurement results under the heading AMB2022-01.

Disclaimer: Certain commercial entities, equipment, or materials may be identified in this document to describe an experimental procedure or concept adequately. Such identification is not intended to imply recommendation or endorsement by the National Institute of Standards and Technology, nor is it intended to imply that the entities, materials, or equipment are necessarily the best available for the purpose.

✉ Maxwell Praniewicz
maxwell.praniewicz@nist.gov

1 Engineering Laboratory, National Institute of Standards and Technology, Gaithersburg, MD 20899, USA

Experimental Procedure

Component Description and Experimental Motivation

The bridge structure parts investigated in this work were produced on the NIST additive manufacturing metrology testbed (AMMT), a NIST-designed and built laser-processing metrology platform, using IN718 powder. Detailed references to the AMMT design, controller, and various other research may be found in [3]. The powder size distribution for the feedstock was characterized by NIST and measurement results are available in [4, 5]. Detailed information on the build including the build layout, part geometry, build parameters, scan strategy, and build conditions can be found in [4]. The part measured was part 2 from build number 7, or the AM-Bench sample designation AMB2022-718-AMMT-B7-P2. No heat treatment was applied to the component. The bridge structure utilized for the part deflection measurements was separated from others on the build plate using electrical discharge machining (EDM). The remaining portion of the build plate left below the bridge component was measured to be 100 mm ± 1 mm long, 11 mm ± 1 mm wide, and 12.5 mm thick. Prior to the measurements on the component, the ridges of the bridge structure were surface ground with minimal material removal to remove the surface texture created by the AM process. This created flat surfaces, which enabled repeatable tactile dimensional measurements on the part. Six ridges on the component were measured using a coordinate measurement machine (CMM) after being surface ground to determine the initial height, $z_{i,\text{initial}}$. The numbering convention of the ridges is defined in Fig. 1. Only these six ridges of the component were selected because they can be easily measured using the substitution method (see following sections). The bridge structure was then separated from the build plate using wire EDM such that only the end portion (under ridge 1 and ridge 2) remains attached. The cut portion of the structure deflected upward from relaxation of the as-built residual stresses. The ridges were then measured again using a CMM to capture the deflected heights, $z_{i,\text{cut}}$. The component deflection for each ridge, δ_i, was then calculated as the difference between the initial and final ridge heights $z_{i,\text{cut}} - z_{i,\text{initial}} = \delta_i$.

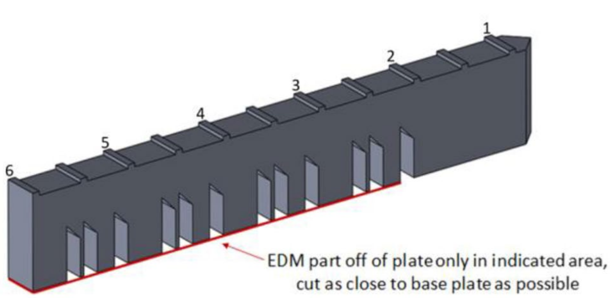

Fig. 1 Bridge component with ridge number definition and indication of EDM cut location

Description of the Substitution Method

To achieve deflection measurements with well-defined uncertainty values, a substitution type measurement approach was utilized. The substitution method (ISO 15530-3 2011) provides "an experimental technique for simplifying the uncertainty evaluation of CMM measurements, whose approach (substitution measurements) leads to measurements being carried out in the same way as actual measurements, but with calibrated workpieces of similar dimension and geometry instead of the unknown workpieces to be measured" [6]. This allows the uncertainty in the measurement of the reference object to be transferred to the measurement of the test object, which in this case is the bridge component, and includes the uncertainty due to the measurement procedure, the uncertainty from the calibration of the calibrated workpiece, and the uncertainty due to the variations of the measured workpieces. This is represented by the following equation where U is the expanded uncertainty of the measurement process given by the summation in quadrature of several factors multiplied by a coverage factor, k:

$$U = k\sqrt{u_{\text{cal}}^2 + u_p^2 + u_b^2 + u_w^2} \tag{1}$$

These factors are the standard uncertainty associated with the calibration of the calibrated workpiece, u_{cal}, the standard uncertainty associated with the measurement procedure, u_p, the standard uncertainty associated with the systematic error of the process, u_b, and the standard uncertainty associated with material and manufacturing variations, u_w.

The reference objects utilized in this work were gage block stacks of various heights wrung together to achieve height values comparable to the anticipated measurement heights. These stacks could comprise of up to three gage blocks. Thus, u_{cal} of the gage block stack would be a combination of the uncertainty of each gage block in the stack. This is defined in Eq. 2, where $U_{\text{cal,GB}i}$ is the uncertainty in the calibration of the ith gage block and k_i is the coverage factor stated on the calibration certificate of the ith gage block.

$$u_{\text{cal}} = \sqrt{\left(\frac{U_{\text{cal,GB1}}}{k_1}\right)^2 + \left(\frac{U_{\text{cal,GB2}}}{k_2}\right)^2 + \left(\frac{U_{\text{cal,GB3}}}{k_3}\right)^2} \tag{2}$$

The uncertainty associated with the measurement procedure includes the repeatability of the measurement process. Thus, u_p is often defined as the standard deviation of repeated measurements utilized. However, the repeatability must be assessed in both the measurement of the reference object, $u_{p,\text{GB}}$, and of the test object, $u_{p,\text{AM}}$. In this work, u_p is defined as the addition in quadrature of the repeatability in these two measurement phases as in Eq. 3. Equations 4 and 5 detail the individual calculations for these values, where n is the number of measurements, y is an individual measurement, and $\overline{y}$ is the average of all measurements.

$$u_p = \sqrt{u_{p,\mathrm{GB}}^2 + u_{p,\mathrm{AM}}^2} \tag{3}$$

$$u_{p,\mathrm{GB}} = \sqrt{\frac{1}{n_{\mathrm{GB}} - 1} \sum_{i=1}^{n_{\mathrm{GB}}} \left(y_{\mathrm{GB},i} - \overline{y_{\mathrm{GB}}}\right)^2} \tag{4}$$

$$u_{p,\mathrm{AM}} = \sqrt{\frac{1}{n_{\mathrm{AM}} - 1} \sum_{i=1}^{n_{\mathrm{AM}}} \left(y_{\mathrm{AM},i} - \overline{y_{\mathrm{AM}}}\right)^2} \tag{5}$$

The uncertainty associated with the systematic error covers any terms which effect the bias of the measurement results. In this work, these are associated with thermal effects. The two terms are associated with these effects include the uncertainty in the coefficient of thermal expansion of the reference objects, $u_{\alpha,\mathrm{GB}i}$, and the uncertainty of the temperature measurement device, u_T. These two terms must be included for all gage blocks used. Thus, u_b is defined in the following equation where T is the temperature, l is the length of the gage block, and α is the coefficient of thermal expansion.

$$u_b = \sqrt{\begin{gathered}\left((T - 20\ {}^\circ\mathrm{C})u_{\alpha,\mathrm{GB1}}l_{\mathrm{GB1}}\right)^2 + \left(\alpha_{\mathrm{GB1}}l_{\mathrm{GB1}}u_T\right)^2 + \left((T - 20\ {}^\circ\mathrm{C})u_{\alpha,\mathrm{GB2}}l_{\mathrm{GB2}}\right)^2 \\ + \left(\alpha_{\mathrm{GB2}}l_{\mathrm{GB2}}u_T\right)^2 + \left((T - 20\ {}^\circ\mathrm{C})u_{\alpha,\mathrm{GB3}}l_{\mathrm{GB3}}\right)^2 + \left(\alpha_{\mathrm{GB3}}l_{\mathrm{GB3}}u_T\right)^2\end{gathered}} \tag{6}$$

The uncertainty associated with manufacturing variations covers terms which differentiate the component from the reference object. In this work, this covers the difference in thermal expansion between the component, u_{wt}, and the reference object and the variation of the surface texture within the object, u_{wp}. The combination of these two terms form u_w.

$$u_w = \sqrt{u_{wt}^2 + u_{wp}^2} \tag{7}$$

The uncertainty associated with the surface texture was calculated from the measurement of the surface texture of the bridge component. The uncertainty associated with differences in the thermal expansion were calculated using the temperature measurements and the uncertainty in the coefficient of thermal expansion.

$$u_{wt} = \sqrt{\left((T - 20\ {}^\circ\mathrm{C})u_{\alpha,\mathrm{AM}}l_{\mathrm{AM}}\right)^2 + \left(\alpha_{\mathrm{AM}}l_{\mathrm{AM}}u_T\right)^2} \tag{8}$$

These terms formed the uncertainty in height measurement using the substitution approach. This was completed to form an uncertainty in the initial height $U_{Zi,\mathrm{initial}}$ and the uncertainty in the final height $U_{Zi,\mathrm{cut}}$. Thus, the uncertainty in the deflection measurement, $U_{\delta,i}$ was calculated as:

$$U_{\delta,i} = k\sqrt{\left(\frac{U_{Z_{i,\mathrm{initial}}}}{k}\right)^2 + \left(\frac{U_{Z_{i,\mathrm{cut}}}}{k}\right)^2} \tag{9}$$

In this experiment, the measurement bias, b, if shown to be repeatable, is assumed to be correctable. Therefore, the bias in the measurements can be calculated as the deviation of the mean value of measurements on the reference object from the true value of the reference.

$$b_{i,\mathrm{initial}} = \overline{x}_{i,\mathrm{initial}} - x_{\mathrm{cal}}, \tag{10}$$

$$b_{i,\mathrm{cut}} = \overline{x}_{i,\mathrm{cut}} - x_{\mathrm{cal}} \tag{11}$$

The final measurement value is the subtraction of the initial from the final values, corrected for bias, with the stated uncertainty value.

$$\delta_i = \left[\left(z_{i,\mathrm{cut}} - b_{i,\mathrm{cut}}\right) - \left(z_{i,\mathrm{initial}} - b_{i,\mathrm{initial}}\right)\right] \pm U_{\delta,i} \tag{12}$$

Description of the Measurand on the Component

To ensure transparency in how the component would be measured, the following geometric dimensioning and tolerancing scheme was chosen for the component. The alignment of the component within the CMM was accomplished using the datum reference frame A, B, C respective to the order of precedence. For the individual ridge measurements, it was chosen not to calculate the height of the ridge relative to datum A. This was due to the anticipated relaxation of the distortion within the build plate. Because of the residual stress within the component, the build plate was bowed. When the component is cut for the deflected measurements, the build plate will also deflect. To minimize the influence of build plate distortion, two datum targets were defined on the areas of the build plate adjacent to the ridges. Thus, the deflection of the ridge is only measured to the adjacent build plate, minimizing the effects of the total distortion of datum A. As depicted, ridge one was measured relative to datum I, ridge two was measured relative to datum H, etc. (Fig. 2).

Description of the Reference Object and Similarity to the Measurand

A requirement of the substitution method is similarity between the reference object and the test object. This includes similarity between the reference object and the test object in terms of the measurand, the measurement procedure, and the environmental conditions. In essence, the measurands evaluated on this component are step heights. Stacks of gage blocks were used to create step heights of

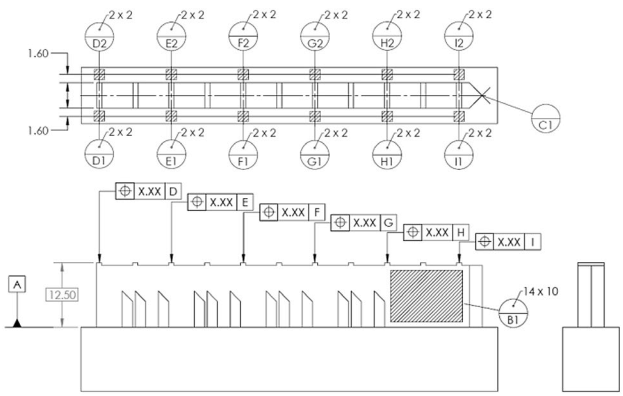

Fig. 2 Definition of the measurement for the AM-Bench component

similar size to the bridge component in both the initial and cut states. This reference object was designed such that it was measured at nominally the same position within the measuring volume of the CMM using a similar measurement procedure.

The gage block stacks were positioned using a spacer such that the measuring area of the block would be nominally in the same lateral position of the ridge to be measured, as shown in Fig. 3. In the initial state, the stacks of gage blocks were all the same nominal height as the bridge object, 12.5 mm. In the cut state, stacks of gage blocks equal in height to the deflected values measured in the 2018 AM-Bench challenge were used as predictions of the deflection. While these may not be the exact values observed here, they will be sufficient to discern if changes in the measured height affect the bias and uncertainty in the component measurement. The step heights were constructed by wringing together several blocks to achieve the appropriate stack height and cross wringing this stack to a base block. The base block was used as the lower plane of the step (shown as datum D comprised of two datum targets in Fig. 3), simulating the base plate of the bridge component, while the wrung blocks were used to simulate the ridges in the bridge component (shown as detail A in Fig. 3). The measurement area on this stack was limited to a 1 mm × 5 mm area to replicate the ridge of the bridge component.

Description of the Measurement Procedure

The measurement of the bridge component and reference object were completed in four stages in order to execute the substitution method for both the initial and cut states of the bridge object. In the first stage, the reference object was measured in the initial configuration. The gage block spacer was placed within the appropriate position of the measurement volume and the gage block stack was placed into position one. The component was then measured using a Giddings and Lewis CORDAX RS-5 CMM equipped with a Renishaw PH10M Probe Head and a Renishaw TP7M Probe. The measurements were performed using a 5 mm/s probing speed and a 1 mm diameter stylus. The coordinate system was located using datums A, B, and C. The reference plane was then measured by probing four points in each datum target zone of the datum surface. Then, six points were probed on the top of the gage block stack within the measurement area. The difference in height between the two planes was calculated by measuring normal to the established datum surface. The reference object was disassembled, and this process was repeated again for a total of eight measurements. This ensured that any potential error induced in fixturing was captured in the repeatability of the process. This procedure was completed again with the gage block stack moved into the next position. This was repeated until all six positions were complete. The temperature was measured during all steps in the measurement procedure.

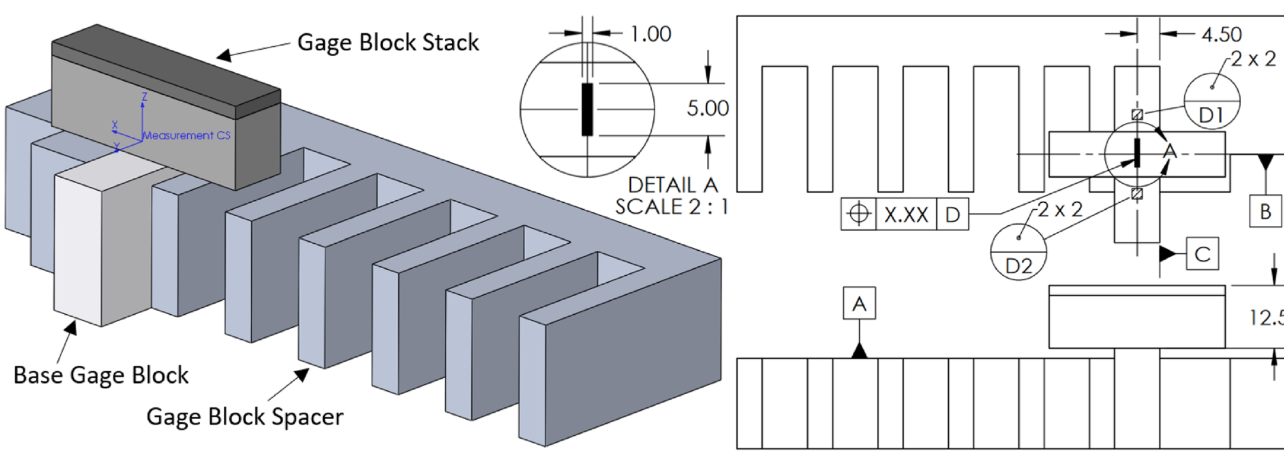

Fig. 3 Reference object and geometry and measurement definition for position one of the reference measurements

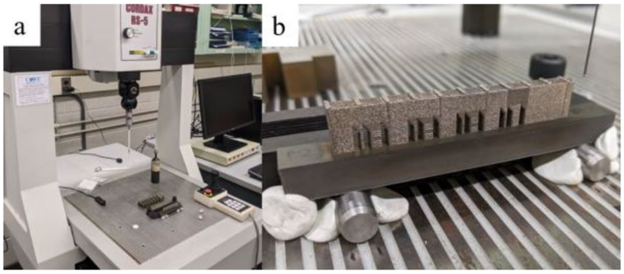

Fig. 4 Setup of the bridge component within the CMM (**a**) and showing a detailed image of fixturing to dowel pins to ensure stability of the component (**b**)

In the second stage, the surface texture of the ridges on the bridge component was first measured using Focus Variation Microscopy. Measurements were performed using an Alicona InfiniteFocus G5 using a 5 × objective having a 0.15 mm numeric aperture. This created a 1.76 µm point spacing for each individual measurement. The system has a 23.5 mm working distance with the 5 × objective, allowing for a large vertical range of the part to be measured at each position. The results from this measurement were used to calculate u_{wp}. After the surface texture measurements were complete, the bridge component was then measured using the CMM in a similar process. The component was aligned within the measurement volume in a position similar to the reference object. The bridge structure was supported on two dowel pins to prevent rocking of the component during the measurement process as shown in Fig. 4. The prescribed datums were used to determine the position of the component within the measurement volume. Each ridge and datum pair were measured with four points per datum target combining for eight points per datum. Six points were measured on the ridge and the height of the ridge was calculated. The remaining five ridges were then measured. The component was then removed, re-fixtured, and measured again. Ten repeat measurements were completed on the bridge component. After the measurements were completed, the component was cut using wire EDM.

In the third stage, the reference object was measured again using the same measurement procedure as described above, but using different heights of gage block stacks in the different positions. The height values used are listed in Table 1. After the measurements of the reference object were completed, the bridge component was measured again in the cut state using the same procedure as described above, concluding stage 4.

Results

Stage 1

The measurement results from stage 1 are shown in Table 2. Both the repeatability and the bias of the measurements are surprisingly good given the rated volumetric accuracy of the CMM. This is largely attributed to the unidirectional nature of the measurements eliminating the lobing effects of the probe. The values for u_p are all under 0.2 µm, indicating very high repeatability of the measurement process, even with the re-fixturing of the component between each replicate measurement. Due to changes in the measurement environment, the temperature increased in the positions that were measured later in the process. Since the measurements were taken at non-standard temperature, the measured mean values were corrected to the expected length at standard temperature. The values for compensation were at most 0.27 µm, and the uncertainty in this value is included in u_b. The bias

Table 1 Heights of height block stacks used in stage 3 of the measurement procedure

	Position 1	Position 2	Position 3	Position 4	Position 5	Position 6
Height (mm)	12.5	12.5	12.64	12.87	13.25	13.77

Table 2 Stage 1 measurement results

	Position 1	Position 2	Position 3	Position 4	Position 5	Position 6
Calibrated height (mm)	12.49999	12.49999	12.49999	12.49999	12.49999	12.49999
u_{cal} (µm)	0.04	0.04	0.04	0.04	0.04	0.04
Mean (mm)	12.4995	12.4999	12.4995	12.4998	12.5000	12.5000
$u_{p,\mathrm{GB}}$ (µm)	0.13	0.16	0.11	0.14	0.15	0.06
T—mean temperature (°C)	18	18	18	19	19	19
Uncertainty in temperature (°C)	1	1	1	1	1	1
u_b—bias uncertainty (µm)	0.12	0.12	0.12	0.12	0.12	0.12
Mean corrected to 20 °C (mm)	12.4998	12.5002	12.4997	12.4999	12.5001	12.5001
b—bias (µm)	− 0.22	0.18	− 0.26	− 0.09	0.11	0.10

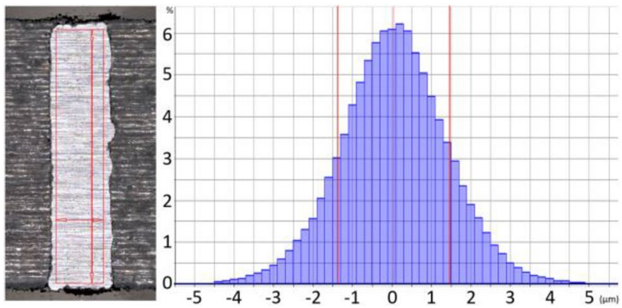

Fig. 5 Surface measurement of bridge object. The left image shows the area analyzed on the ridge, marked by the red rectangle. The right image shows the distribution of surface heights within the measurement area

between the measured values and the calibrated gage block stacks were again very low compared to what was expected. The largest bias value observed was −0.26 µm, indicating good agreement between the calibrated value and the measurements performed by the CMM. These results indicate good performance of the measurement system, allowing for progression to stage 2.

Stage 2

The results of the surface texture measurement of one ridge of the bridge component are shown in Fig. 5. Instead of calculating parameters to describe the roughness of the surface, (such as Sa or Sq) and deriving a value for the uncertainty due to the surface roughness, the distribution of the surface texture was directly analyzed. The standard uncertainty associated with variations in surface texture, u_{wp}, was chosen as one standard deviation of the distribution of surface variation within the measurement area on the ridge of the ridge component, which is shown to be normal in Fig. 5. This resulted in a u_{wp} value of 1.5 µm.

The results from the stage 2 CMM measurements are shown in Table 3. The low values of $u_{p,\mathrm{AM}}$ once again indicate a very repeatable measurement process, with all values under 0.3 µm. While the temperature remained stable throughout these measurements, they remained below 20 °C. Thus, these values again needed correction to the reference temperature. The contribution from surface texture is clearly the largest contributor to the uncertainty, with the u_{wp} value of 1.5 µm.

Table 4 presents the standard uncertainties combined in quadrature to form the final measurement uncertainty, U, and the measured value, Y. Clearly, the measurement uncertainty is dominated by the contribution of surface texture, leading to a u_w of 1.51 µm. The expanded uncertainty ($k = 2$) for all ridges was calculated to be 3 µm. The height of ridges one through six were measured to have a range of 0.185 mm. The variation in ridge heights can be observed to be largely parabolic in Fig. 6. While all ridges were surface ground to lie within the same plane, the build plate was significantly warped due to the residual

Table 3 Stage 2 measurement results

	Ridge 1	Ridge 2	Ridge 3	Ridge 4	Ridge 5	Ridge 6
Mean (mm)	11.9761	12.1033	12.1617	12.1602	12.1005	11.9940
$u_{p,\mathrm{AM}}$ (µm)	0.13	0.20	0.26	0.10	0.17	0.20
T—mean temperature (°C)	18	18	18	18	18	18
Uncertainty in temperature (°C)	1	1	1	1	1	1
Mean corrected to 20 °C (mm)	11.9765	12.1037	12.1620	12.1605	12.1008	11.9943
u_{wt} (µm)	0.16	0.16	0.16	0.16	0.16	0.16
u_{wp} (µm)	1.50	1.50	1.50	1.50	1.50	1.50

Table 4 Initial bridge component measurement results

	Ridge 1	Ridge 2	Ridge 3	Ridge 4	Ridge 5	Ridge 6
u_{cal} (µm)	0.04	0.04	0.04	0.04	0.04	0.04
u_b (µm)	0.12	0.12	0.12	0.12	0.12	0.12
u_w (µm)	1.51	1.51	1.51	1.51	1.51	1.51
u_p (µm)	0.19	0.26	0.28	0.18	0.22	0.21
$z_{i,\mathrm{initial}}$ (mm)	11.9767	12.1035	12.1623	12.1606	12.1007	11.9942
$\pm U_{z_{i,\mathrm{initial}}}$ (mm)	0.0030	0.0031	0.0031	0.0030	0.0031	0.0031

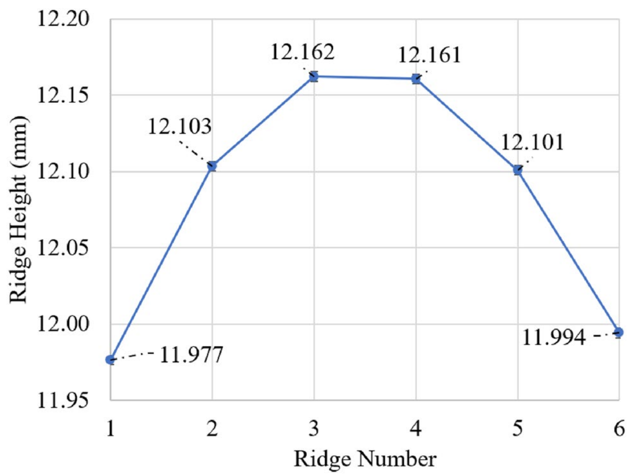

Fig. 6 Initial bridge component height measurements

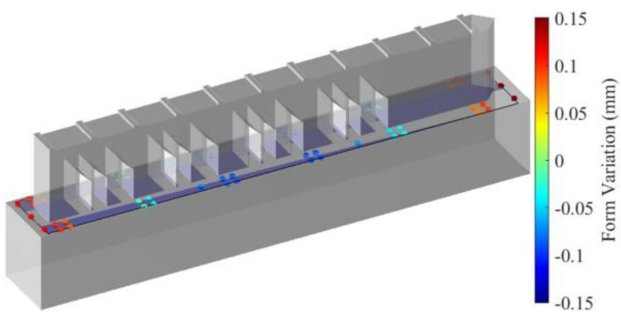

Fig. 7 Form variation on build plate in the initial state

stress accumulated within the component during the build process. Figure 7 displays this form variation in the build plate. The ends of the plate are bowed upward and the total form error (of the points measured) was measured to be 0.246 mm.

Stage 3

Table 5 shows the stage 3 measurement results. Since different gage block stacks were required for this stage, different values of u_{cal} were utilized. However, the uncertainty in the height of the gage block stacks were all sufficiently low. The values for all gage block stacks and the uncertainty values are recorded in Table 10 in the Appendix. Some differences in the repeatability are observed between the stage 1 and stage 3 results. The repeatability of some positions has improved (2, 3, 6), while others have degraded (1, 4, 5). However, the largest change was found to only be 0.1 µm. Again, the temperature was stable, but below standard temperature. Changes in the bias can also be observed. The largest bias change between stage 1 and 3 was 0.27 µm in position 2.

Stage 4

Table 6 shows the results of the stage 4 measurements. Environmental control was restored for this stage of the measurements and all measurements were taken at standard reference temperature. Thus, the measured values did not need

Table 5 Stage 3 measurement results

	Position 1	Position 2	Position 3	Position 4	Position 5	Position 6
Calibrated Height (mm)	12.49999	12.49999	12.63999	12.87002	13.2501	13.77005
u_{cal} (µm)	0.04	0.04	0.07	0.07	0.07	0.06
Mean (mm)	12.4997	12.4996	12.6395	12.8697	13.2498	13.7699
$u_{p,GB}$ (µm)	0.20	0.13	0.04	0.21	0.25	0.03
T—mean temperature (°C)	18	18	18	18	18	18
Uncertainty in temperature (°C)	1	1	1	1	1	1
u_b—bias uncertainty (µm)	0.12	0.12	0.12	0.12	0.12	0.12
Mean corrected to 20 °C (mm)	12.49995	12.49990	12.63979	12.86997	13.25004	13.77021
b—bias (µm)	−0.04	−0.09	−0.20	−0.05	−0.06	0.16

Table 6 Stage 4 measurement results

	Ridge 1	Ridge 2	Ridge 3	Ridge 4	Ridge 5	Ridge 6
Mean (mm)	11.9742	12.1188	12.3447	12.6837	13.1590	13.8032
$u_{p,AM}$ (µm)	0.14	0.18	0.14	0.12	0.16	0.29
T—mean temperature (°C)	20	20	20	20	20	20
Uncertainty in temperature (°C)	1	1	1	1	1	1
u_{wt} (µm)	0.16	0.16	0.16	0.17	0.17	0.18
u_{wp} (µm)	1.50	1.50	1.50	1.50	1.50	1.50

Table 7 Cut bridge component measurement results

	Ridge 1	Ridge 2	Ridge 3	Ridge 4	Ridge 5	Ridge 6
u_{cal} (µm)	0.04	0.04	0.07	0.07	0.07	0.06
u_b (µm)	0.12	0.12	0.12	0.12	0.12	0.12
u_w (µm)	1.51	1.51	1.51	1.51	1.51	1.51
u_p (µm)	0.24	0.22	0.15	0.24	0.29	0.30
$z_{i,cut}$ (mm)	11.9742	12.1189	12.3449	12.6838	13.1590	13.8030
$\pm U_{z_{i,cut}}$ (mm)	0.0031	0.0031	0.0030	0.0031	0.0031	0.0031

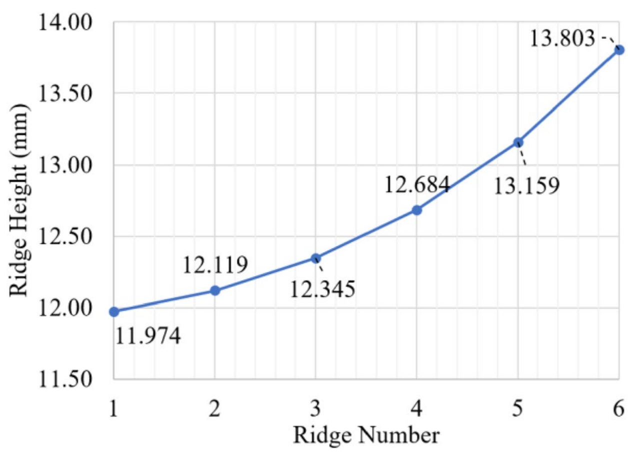

Fig. 8 Cut bridge component height measurements

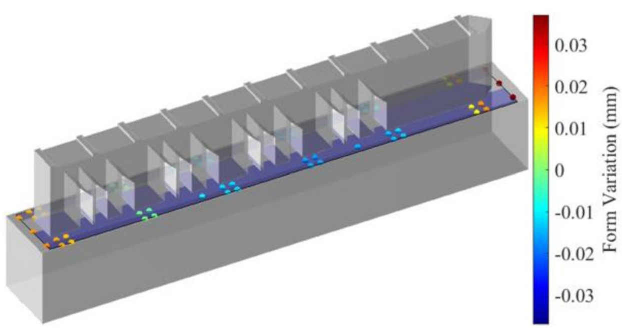

Fig. 9 Form variation on build plate in the cut state

correction. The repeatability of this stage is also comparable to the results observed in stage 2.

Table 7 presents the uncertainties in the stage 4 measurement results. Again, the measurement uncertainty is dominated by the surface texture, u_w. Despite changes in u_{cal} and u_p, the expanded uncertainty ($k = 2$) is very similar between the initial and cut measurements. The heights of the ridges clearly have deflected upward with the release of the residual stress. This is shown in Fig. 8. The influence of the build plate deflection is less apparent in the cut state, as the trend is dominated by the deflection. Figure 9 displays the form variation of the build plate in the as cut state. The form error of the measured points was 0.053 mm, showing significant relaxation of the build plate.

Deflection Measurements

Table 8 presents the final deflection measurement results. Through the combination in quadrature of the two combined standard uncertainties multiplied by the coverage factor ($k = 2$), the final uncertainty in the deflection measurements for all ridges was calculated to be 4.3 µm. The deflection measurement results are also shown in Fig. 10. As expected, minimal deflection is observed in ridges one and two, with the measured deflection in ridge one being within the uncertainty bounds. The remaining ridges follow a parabolic upward deflection.

Table 8 Deflection measurement results

	Ridge 1	Ridge 2	Ridge 3	Ridge 4	Ridge 5	Ridge 6
δ_i (mm)	−0.0025	0.0154	0.1826	0.5232	1.0583	1.8088
$\pm U(\delta_i)$ (mm)	0.0043	0.0043	0.0043	0.0043	0.0043	0.0043

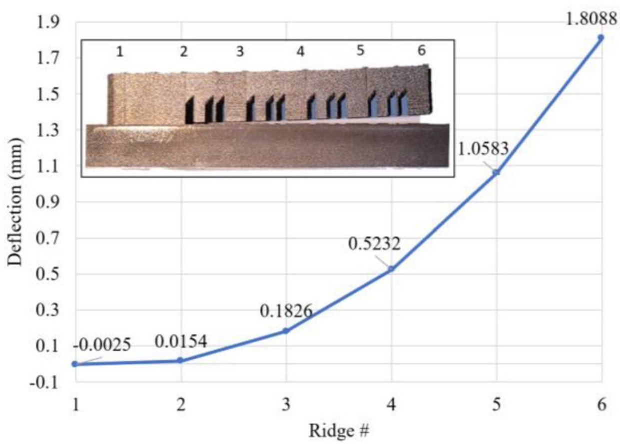

Fig. 10 Deflection measurement results

Conclusion

This work presented a complete description of the measurement methodology and results of the CHAL-AMB2022-01-PD. Care was taken to provide a well-defined measurand for the challenge to allow comparability between simulation results. A rigorous methodology was implemented to quantify the uncertainty in the height measurement of the bridge component. The final deflection results are presented with a well quantified uncertainty value.

Appendix

See Tables 9 and 10.

Table 9 Stage 1 gage block stacks

	Ridge 1	Ridge 2	Ridge 3	Ridge 4	Ridge 5	Ridge 6
GB 1						
Nominal height (mm)	10.50	10.50	10.50	10.50	10.50	10.50
Bias (µm)	−0.01	−0.01	−0.01	−0.01	−0.01	−0.01
Uncertainty ($k=2$) (µm)	0.07	0.07	0.07	0.07	0.07	0.07
CTE (mm/(mm K))	1.08E−05	1.08E−05	1.08E−05	1.08E−05	1.08E−05	1.08E−05
CTE uncertainty	5.40E−07	5.40E−07	5.40E−07	5.40E−07	5.40E−07	5.40E−07
GB 2						
Nominal height (mm)	2.0	2.0	2.0	2.0	2.0	2.0
Bias (µm)	0.00	0.00	0.00	0.00	0.00	0.00
Uncertainty ($k=2$) (µm)	0.06	0.01.08E−05	0.06	0.06	0.06	0.06
CTE (mm/(mm K))	1.08E−05	6	1.08E−05	1.08E−05	1.08E−05	1.08E−05
CTE uncertainty	5.40E−07	5.40E−07	5.40E−07	5.40E−07	5.40E−07	5.40E−07
Calibrated height (mm)	12.49999	12.49999	12.49999	12.49999	12.49999	12.49999
u_{cal} (µm)	0.04	0.04	0.04	0.04	0.04	0.04

Table 10 Stage 3 gage block stacks

	Ridge 1	Ridge 2	Ridge 3	Ridge 4	Ridge 5	Ridge 6
GB 1						
Nominal height (mm)	10.50	10.50	10.50	10.50	10.50	10.50
Bias (µm)	−0.01	−0.01	−0.01	−0.01	−0.01	−0.01
Uncertainty (k=2) (µm)	0.07	0.07	0.07	0.07	0.07	0.07
CTE (mm/(mm K))	1.08E−05	1.08E−05	1.08E−05	1.08E−05	1.08E−05	1.08E−05
CTE uncertainty	5.40E−07	5.40E−07	5.40E−07	5.40E−07	5.40E−07	5.40E−07
GB 2						
Nominal height (mm)	2.00	2.00	1.00	1.00	1.25	2.00
Bias (µm)	0.00	0.00	0.00	0.00	0.05	0.00
Uncertainty (k=2) (µm)	0.06	0.06	0.08	0.08	0.08	0.06
CTE (mm/(mm K))	1.08E−05	1.08E−05	1.08E−05	1.08E−05	1.08E−05	1.08E−05
CTE uncertainty	5.40E−07	5.40E−07	5.40E−07	5.40E−07	5.40E−07	5.40E−07
GB 3						
Nominal height (mm)			1.14	1.37	1.5	1.27
Bias (µm)			0.00	0.03	0.06	0.06
Uncertainty (k=2) (µm)			0.08	0.08	0.08	0.08
CTE (mm/(mm K))			1.08E−05	1.08E−05	1.08E−05	1.08E−05
CTE uncertainty			5.40E−07	5.40E−07	5.40E−07	5.40E−07
Calibrated height (mm)	12.49999	12.49999	12.63999	12.87002	13.25010	13.77005
u_{cal} (µm)	0.04	0.04	0.07	0.07	0.07	0.06

Acknowledgements The authors would like to thank Eric Stanfield of the Dimensional Metrology Group at NIST for sharing some of his vast knowledge on the handling and measurement of gage blocks to inform the development of the measurement process.

Funding Funding was provided by NIST (Grant No. STRS Funding).

Declarations

Conflict of interest On behalf of all authors, the corresponding author states that there is no conflict of interest.

References

1. Bartlett JL, Li X (2019) An overview of residual stresses in metal powder bed fusion. Addit Manuf 27:131–149. https://doi.org/10.1016/j.addma.2019.02.020
2. Levine L et al (2022) Outcomes and conclusions from the 2022 AM-Bench measurements, challenge problems, modeling submissions, and conference
3. NIST (2023) AMMT-TEMPS/relevant publications. https://www.nist.gov/el/ammt-temps/relevant-publications. Accessed 05 July 2023
4. NIST (2022) AMB2022-01 benchmark measurements and challenge problems. NIST additive manufacturing benchmark test series (AM-Bench). https://www.nist.gov/ambench/amb2022-01-benchmark-measurements-and-challenge-problems. Accessed 22 Dec 2022
5. Whiting JG, Tondare VN, Scott JHJ, Phan TQ, Donmez MA (2019) Uncertainty of particle size measurements using dynamic image analysis. CIRP Ann 68(1):531–534. https://doi.org/10.1016/j.cirp.2019.04.075
6. International Organization for Standardization (2011) ISO 15530–3:2011 Geometrical product specifications (GPS)—coordinate measuring machines (CMM): technique for determining the uncertainty of measurement—part 3: use of calibrated workpieces or measurement standards. ISO, Geneva